nature neuroscience

ARTICLES

A readily retrievable pool of synaptic vesicles

Yunfeng Hua[1,2,7], Raunak Sinha[1,2,7], Cora S Thiel[1,2,7], Roman Schmidt[3], Jana Hüve[2,4], Henrik Martens[5], Stefan W Hell[3], Alexander Egner[3,6] & Jurgen Klingauf[1,2,4]

Although clathrin-mediated endocytosis is thought to be the predominant mechanism of synaptic vesicle recycling, it seems to be too slow for fast recycling. Therefore, it was suggested that a presorted and preassembled pool of synaptic vesicle proteins on the presynaptic membrane might support a first wave of fast clathrin-mediated endocytosis. In this study we monitored the temporal dynamics of such a 'readily retrievable pool' of synaptic vesicle proteins in rat hippocampal neurons using a new type of probe. By applying cypHer5E, a new cyanine dye–based pH-sensitive exogenous marker, coupled to antibodies to luminal domains of synaptic vesicle proteins, we could reliably monitor synaptic vesicle recycling and demonstrate the preferential recruitment of a surface pool of synaptic vesicle proteins upon stimulated endocytosis. By using fluorescence nanoscopy of surface-labeled synaptotagmin 1, we could resolve the spatial distribution of the surface pool at the periactive zone in hippocampal boutons, which represent putative sites of endocytosis.

A main rate-limiting step in synaptic transmission is the retrieval of synaptic vesicles from the presynaptic membrane for further rounds of use. Several modes of synaptic vesicle retrieval have been proposed, but the main pathway is considered to be clathrin-mediated endocytosis[1,2]. This process is relatively slow because after fusion the recycling machinery has to resort different vesicle membrane proteins in the right stoichiometry to generate fusion-competent synaptic vesicles[3]. As a result, this process occurs with a time constant of tens of seconds to minutes[4]. However, to sustain transmission during continuous activity, it was suggested that synaptic vesicles might 'kiss and run' with a time constant of 1–2 s, whereby the vesicles transiently fuse with the membrane without full collapse and hence retain their molecular identity[5–9].

The fast 'kiss and run' recycling mechanism not only would provide a kinetic advantage but would spatially and temporally couple exo- and endocytosis. Using a green fluorescent protein (GFP) fused with the coat-forming clathrin light chain, we previously found evidence that during the first 10 s of prolonged stimulation, clathrin is not being recruited from the cytosol to form coated pits, although the rate of endocytosis measured with styryl (FM) dyes is high[3], suggesting that vesicles during this first phase are either retrieved by a clathrin-independent mechanism (kiss and run) or by preassembled coat structures at the periphery of the active zone.

Support for such a 'readily retrievable pool' (RRetP) of preassembled structures came from experiments using fusion constructs of the synaptic vesicle proteins synaptobrevin 2 (Syb2) and synaptotagmin 1 (Syt1) with a pH-sensitive GFP, pHluorin[10]. These studies showed that synaptic vesicles lose their protein complement after fusion, and the molecular identity of synaptic vesicles exocytosed and subsequently endocytosed is not conserved[11–13]. On the basis of these observations, we suggested that exocytosis and subsequent endocytosis are uncoupled and that there is a pool of preassembled vesicle proteins on the presynaptic surface that is preferentially retrieved on exocytosis[3,13]. Previous studies using activity-dependent markers in snake neuromuscular terminals have proposed that the accumulation of such probes at the bouton margins upon stimulation might represent endocytic active zones[14,15]. This is in agreement with other ultrastructural and high-resolution microscopy analyses that describe the presence of several synaptic vesicle proteins on the presynaptic membrane of resting synapses[16,17]. Likewise, the first reconstruction of the endocytic time course from electron micrographs of frog neuromuscular junctions quick-frozen at different times after stimulation revealed a first wave of clathrin-mediated endocytosis lasting ~10 s (ref. 18), in line with the notion of a preclustered pool being immediately available for this first wave of endocytosis upon stimulation[13]. In hippocampal boutons, transient overexpression of the genetic exo-endocytic probe synaptopHluorin (spH)[10], in which pHluorin is fused to the luminal domain of Syb2, leads to targeting of up to ~30% of spH to the bouton membrane, constituting a surface pool that participates in synaptic vesicle protein recycling during compensatory endocytosis[11,13].

However, the discovery that expressed pHluorin-tagged versions of other synaptic vesicle proteins are found to only a minor extent on the surface—only about 8% of total synaptophysin-pHluorin[2] is found on the surface, and only about 2% of the glutamate transporter vGlut1-pHluorin[19]—has called into question the existence of a surface pool of endogenous synaptic vesicle proteins. The high surface expression of spH and Syt1-pHluorin[11,13] might be a mere overexpression artifact, thus discrediting the use of pHluorins as optical probes for exo-endocytosis[17]. Endogenous synaptic vesicle proteins might be only transiently exposed to the surface during exo-endocytosis and might even remain clustered, thereby tightly coupling exo- and

[1]Department of Membrane Biophysics, Max Planck Institute for Biophysical Chemistry, Goettingen, Germany. [2]Department of Cellular Biophysics, Institute of Medical Physics and Biophysics, University of Muenster, Muenster, Germany. [3]Department of NanoBiophotonics, Max Planck Institute for Biophysical Chemistry, Goettingen, Germany. [4]Fluorescence Microscopy Facility Muenster, Center for Nanotechnology (CeNTech), Muenster, Germany. [5]Synaptic Systems GmbH, Goettingen, Germany. [6]Current address: Laser-Laboratorium Goettingen e.V., Goettingen, Germany. [7]These authors contributed equally to this work. Correspondence should be addressed to J.K. (klingauf@uni-muenster.de).

Received 15 November 2010; accepted 14 April 2011; published online 12 June 2011; doi:10.1038/nn.2838

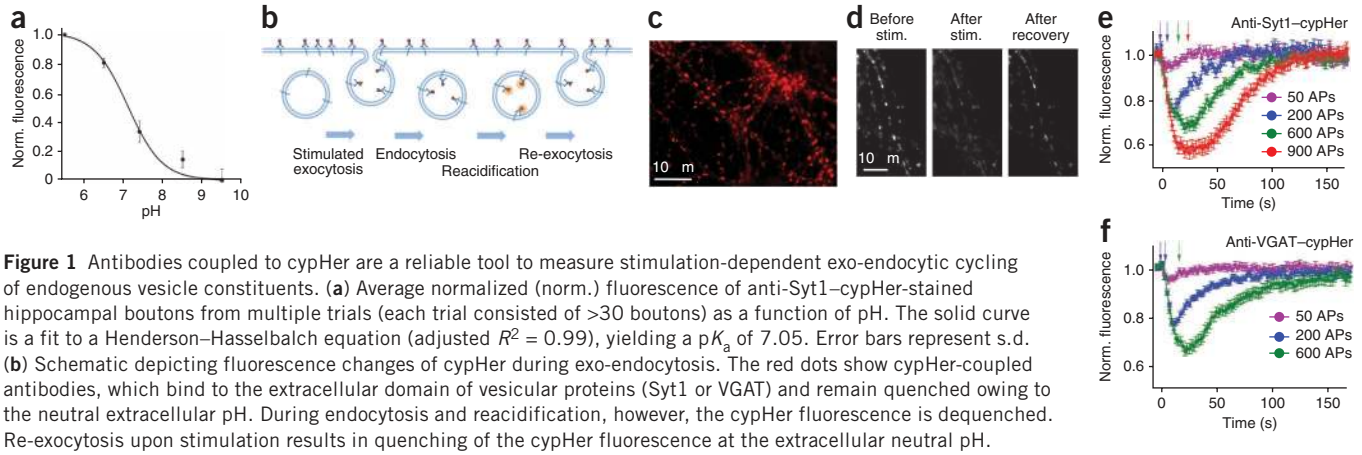

Figure 1 Antibodies coupled to cypHer are a reliable tool to measure stimulation-dependent exo-endocytic cycling of endogenous vesicle constituents. (**a**) Average normalized (norm.) fluorescence of anti-Syt1–cypHer-stained hippocampal boutons from multiple trials (each trial consisted of >30 boutons) as a function of pH. The solid curve is a fit to a Henderson–Hasselbalch equation (adjusted $R^2 = 0.99$), yielding a pK_a of 7.05. Error bars represent s.d. (**b**) Schematic depicting fluorescence changes of cypHer during exo-endocytosis. The red dots show cypHer-coupled antibodies, which bind to the extracellular domain of vesicular proteins (Syt1 or VGAT) and remain quenched owing to the neutral extracellular pH. During endocytosis and reacidification, however, the cypHer fluorescence is dequenched. Re-exocytosis upon stimulation results in quenching of the cypHer fluorescence at the extracellular neutral pH. (**c**) Fluorescence image of hippocampal neurons labeled with anti-VGAT–cypHer. The label forms a punctate pattern with puncta typically representing individual boutons. (**d**) Fluorescence images of hippocampal neurons stained with anti-VGAT–cypHer before and directly after application of a stimulus (stim.) of 900 action potentials (APs) and 100 s later. (**e**) Average normalized fluorescence transient of anti-Syt1–cypHer-stained boutons in response to different action potential trains at 20 Hz ($n = 3$ experiments with >50 boutons for each). Traces were corrected for photobleaching. Error bars represent s.e.m. (**f**) Average normalized fluorescence transient of anti-VGAT–cypHer-stained boutons in response to different action potential trains at 20 Hz ($n = 3$ experiments with >50 boutons for each). Traces were corrected for photobleaching. Error bars represent s.e.m.

endocytosis[17]. Thus, it is crucial to directly visualize spatially and temporally the retrieval of endogenous synaptic vesicle proteins from an RRetP of synaptic vesicles, if it exists.

In this study we used a new pH-sensitive fluorophore, cypHer5E[20,21] (referred to here as cypHer), which has a pH dependence that is opposite to that of pHluorin. The cypHer fluorophore was coupled to antibodies to the luminal domains of Syt1 (anti-Syt1–cypHer) and to vesicular GABA transporter (VGAT) (anti-VGAT–cypHer[21]); Syt1 and VGAT are two endogenous synaptic vesicle proteins that, when overexpressed as pHluorin-tagged versions, either show very high or are expected to show very little surface expression, respectively. By using these new probes in combination with spH[10], we were able to visualize in real time the retrieval of endogenous Syt1 and VGAT from the surface RRetP of synaptic vesicles[13]. The existence of an RRetP was further substantiated by 4Pi microscopy[22,23] and isoSTED (isotropic stimulated emission depletion)[24] imaging of surface Syt1, which revealed a doughnut-like arrangement of Syt1 patches around the active zone and postsynaptic density (PSD) complexes visualized by immunostaining for the cytomatrix at the active zone (CAZ) components RIM1 (regulating synaptic membrane exocytosis protein 1; also known as RIMS1) and RIM2 (also known as RIMS2) and the PSD scaffolding protein Homer1. This is in agreement with previous studies in *Drosophila melanogaster* neuromuscular junction and other synaptic preparations in which endocytic 'hot spots' are located at the periactive zone[14,15,25–27].

RESULTS

Exo-endocytosis of endogenous synaptic vesicle proteins

For characterizing the pH dependence of the fluorescence of cypHer-coupled antibodies, cultured hippocampal neurons were labeled with anti-Syt1–cypHer by incubation at 37 °C for 3–4 h (see Online Methods), then fixed, permeabilized and superfused with buffers of different pH. The fluorescence was maximal at pH 5.5 and minimal at pH 9 (**Fig. 1a**). Normalized fluorescences ($\Delta F/F$) could be fit by the Henderson–Hasselbalch equation (**Fig. 1a**), yielding a pK_a value of 7.05, which is ideal to measure pH changes during exo- and endocytosis[28].

For measuring presynaptic activity, we labeled live hippocampal neurons with either anti-Syt1–cypHer or anti-VGAT–cypHer as above (**Fig. 1b**). During vesicle recycling these antibodies bind to their specific epitopes and are internalized (**Fig. 1c**). In the acidic vesicular lumen, protonated cypHer molecules emit red fluorescence when excited at 640 nm, whereas cypHer-tagged molecules on the presynaptic membrane are sufficiently quenched at pH 7.4, leading to a punctate staining. As spontaneous action potentials were not blocked during labeling, antibody uptake into synaptic vesicles was primarily mediated by spontaneous activity. To assess the efficiency of this labeling strategy, we stained neurons with anti-Syt1–cypHer by eliciting 900 action potentials at 20 Hz, a stimulus that was shown to deplete the entire recycling pool of synaptic vesicles in hippocampal boutons[29]. Neurons were then incubated at 37 °C for 5–10 min followed by extensive washing to remove unbound antibodies. We next estimated the internalized fraction of cypHer for both staining protocols by quenching their fluorescence with NH_4Cl (50 mM), which equilibrates the pH across all membranes and therefore unmasks any cypHer inside acidic compartments[29]. This quenchable fraction, which represents the amount of anti-Syt1–cypHer internalized into synaptic vesicles, is comparable for both staining protocols (**Supplementary Fig. 1**); however, the stimulation-independent procedure with long incubation time (3–4 h) labels a larger fraction of synaptic vesicles (**Supplementary Fig. 1**). We next tested the efficiency of this probe to report stimulation-dependent exo-endocytosis. Trains of action potentials were evoked by electric field stimulation at 20 Hz, resulting in a rapid decay of cypHer fluorescence at individual boutons owing to quenching of vesicular cypHer upon fusion at the external pH of 7.4 (**Fig. 1d**). After cessation of stimulation, cypHer-coupled antibodies were retrieved by compensatory endocytosis and dequenched during reacidification of the vesicle lumen (**Fig. 1e**). Of note, inhibitory boutons labeled by anti-VGAT–cypHer showed near-identical stimulation-dependent fluorescence transients for different stimulus strengths (**Fig. 1f**). Labeling with cypHer provides a fluorescence signal that is the reverse of that provided by labeling with spH, as expected from its reverse pH sensitivity. However, the cypHer dye is less photostable than spH, making correction for photo-bleaching necessary (**Supplementary Fig. 2**; see Online Methods) when not using a back-illuminated charge-coupled device (CCD).

Size of the surface pool of synaptic vesicle constituents

As for spH, cypHer fluorescence changes scale with the stimulus strength for boutons labeled with anti-Syt1–cypHer and boutons

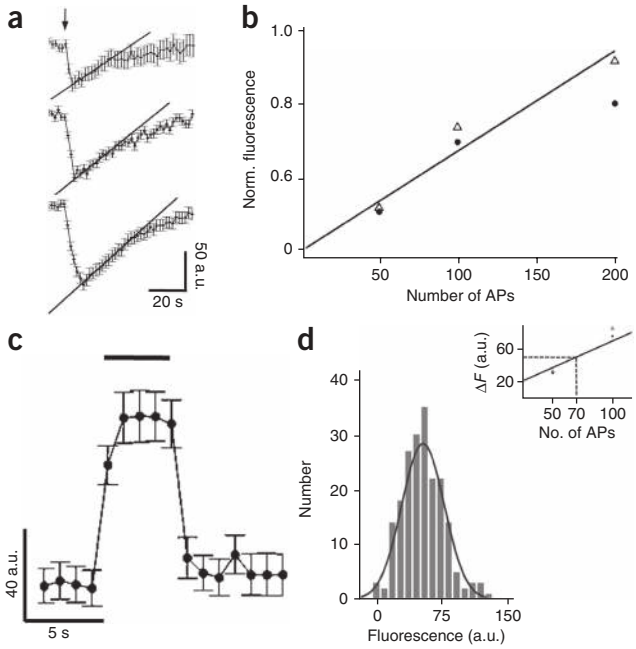

Figure 2 Dose–response curve to analyze the size of the surface pool. (**a**) Averaged fluorescence transients of anti-Syt1–cypHer-stained boutons in response to 50, 100 and 200 action potentials at 20 Hz ($n = 5$ experiments with >50 boutons for each). Lines were fitted to the initial fluorescence recovery phases to estimate the endocytic rate constant during stimulation. Back-extrapolation to zero yields the exocytosis amplitudes. Error bars represent s.e.m. (**b**) Average peak changes in normalized (norm.) fluorescence (ΔF) plotted as a function of action potential number (filled circles) together with ΔF values corrected for endocytosis during stimulation (triangles) by back-extrapolation (**a**). These data points lie close to a line fit. (**c**) Average fluorescence response to an acid pulse of boutons labeled with anti-Syt1–cypHer, yielding the size of the surface pool. Error bars represent s.e.m. (**d**) Distribution of bouton fluorescence responses to an acid pulse. The solid black line is a Gaussian fit (adjusted $R^2 = 0.99$) yielding a mean size of 49.46 ± 1.56 a.u. Inset, mean size of the surface pool estimated by the acid pulse is equivalent to the absolute fluorescence change triggered by 70 action potentials (APs).

labeled with anti-VGAT–cypHer (**Fig. 1e**,**f**), and the peak fluorescences report the net difference between the kinetics of exo- and endocytosis during stimulation. However, previous studies based on spH have shown that the initial rate of endocytosis after stimulus is similar to the endocytic rate during the stimulus period[29,30]. Thus, we could estimate the pure exocytosis amplitude ΔF by back-extrapolating a linear fit to the initial post-stimulus rate of endocytosis (**Fig. 2a**). Back-extrapolated ΔF values, which are proportional to the numbers of released synaptic vesicles, rise linearly with stimulus strength (**Fig. 2b**), as shown previously for spH[29,30].

Up to ~30% of overexpressed spH is stranded on the synaptic membrane upon overexpression in hippocampal boutons[12,13,29]. It has been shown, however, that endogenous synaptic vesicle proteins also are present on the membrane[16,17]. To readdress this issue we superfused anti-Syt1–cypHer-labeled boutons with buffer of pH 5.5 to selectively visualize the presynaptic surface pool (**Fig. 2c**,**d**). The size distribution of surface fluorescences from individual boutons fitted well with a Gaussian distribution (adjusted squared correlation coefficient $R^2 = 0.98$) with a mean of 49.46 ± 1.56 arbitrary units (a.u.). The size of this total surface pool corresponds to a fluorescence change induced by ~70 action potentials (**Fig. 2d**, inset). This indicates that the surface pool might be capable of supporting compensatory endocytosis of synaptic vesicles for stimuli of up to 70 action potentials—that is, it is similar in size to the readily releasable pool (RRP) of docked and primed vesicles[31–33].

Labeled antibodies report same recycling kinetics as spH

Next, we labeled hippocampal neurons overexpressing the genetically encoded pH sensor spH with the cypHer-coupled antibodies and performed dual-color imaging. Because of the wide spectral separation, no bleed-through was observed. Functional spH-expressing boutons were colabeled with anti-Syt1–cypHer (**Fig. 3a**). As the spH transfection efficiency is only ~10%, not all anti-Syt1–cypHer-stained boutons coexpress spH. We next examined the fluorescence changes in response to 200 action potentials at 20 Hz (**Fig. 3a**). SpH and anti-Syt1–cypHer responses of the same boutons showed mirror-image signals with near-identical endocytic time constants for monoexponential fits (~23 s versus ~22 s). This indicates that both reporters—an overexpressed and an exogenous probe—reliably report exo-endocytosis and do not artificially affect synaptic vesicle recycling.

For specifically investigating the recycling kinetics of the inhibitory synapses, we labeled spH-transfected boutons using anti-VGAT–cypHer (**Fig. 3b**). A ~32% fraction of all spH-expressing boutons could be stained with anti-VGAT–cypHer, representing the fraction of inhibitory synapses in our cultures. Stimulation with 200 action potentials at 20 Hz induced similar fluorescence transients (~22 s exponential endocytic time constant) in both channels (**Fig. 3b**). Therefore, the kinetics of endocytosis and reacidification in inhibitory synapses are indistinguishable from the whole population response as probed with spH and anti-Syt1–cypHer.

A surface RRetP of synaptic vesicle constituents

Previous studies have shown that synaptic vesicle proteins are also resident on the bouton membrane and that these surface proteins

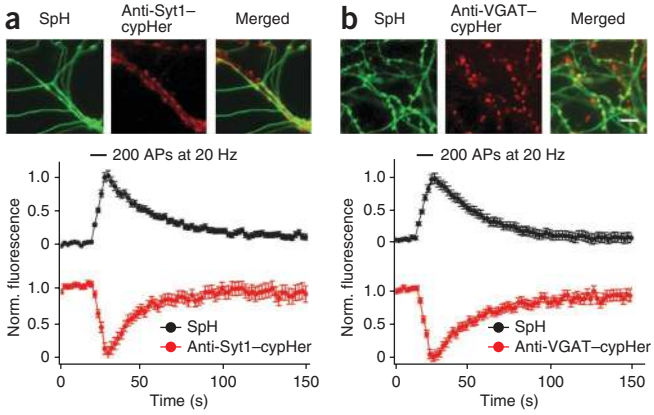

Figure 3 Comparison of vesicle recycling kinetics probed with synaptopHluorin and cypHer-coupled antibodies. (**a**) Top: staining of spH-transfected hippocampal neurons with anti-Syt1–cypHer. Fluorescence images show colocalization of individual boutons expressing spH (green) with endogenous Syt1 (red) labeled with anti-Syt1–cypHer. Bottom: average fluorescence transients of double-labeled boutons in response to 200 action potentials at 20 Hz ($n = 5$ experiments with >50 boutons for each). Traces were corrected for photobleaching. Error bars represent s.e.m. (**b**) Top: staining of spH-transfected hippocampal neurons with anti-VGAT–cypHer. Fluorescence images show colocalization of individual boutons expressing spH (green) with the inhibitory synapse marker VGAT (red). Bottom: average fluorescence transients of double-labeled boutons in response to 200 action potentials (APs) at 20 Hz ($n = 5$ experiments with >50 boutons for each). Traces were corrected for photobleaching. Error bars represent s.e.m. Scale bars represent 5 μm.

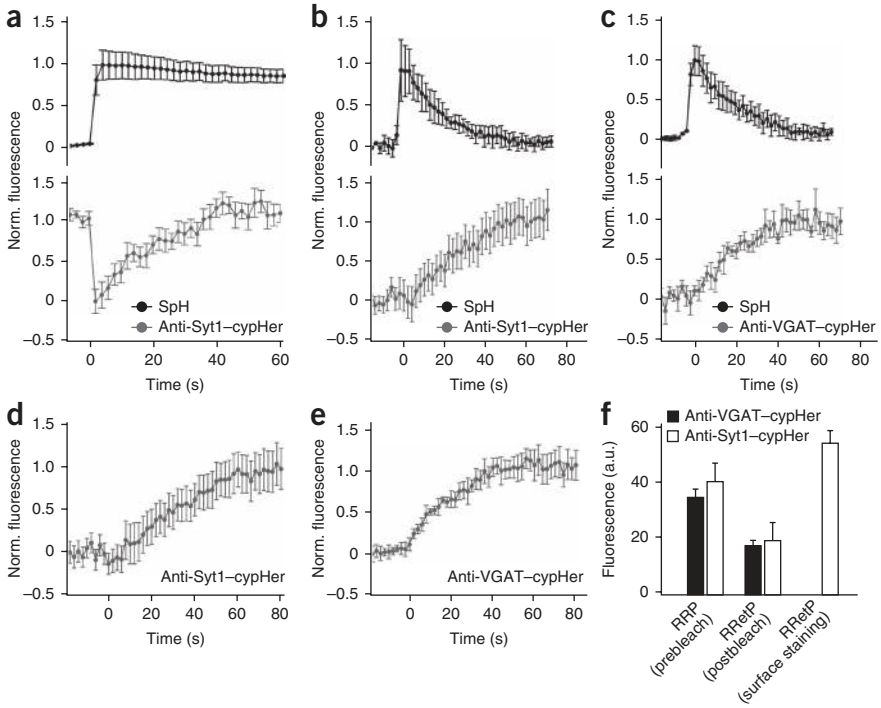

Figure 4 Readily retrievable surface pool of synaptic vesicle constituents. (**a**) Cleaving membrane-stranded spH with TEV protease does not affect the cypHer signal at anti-Syt1–cypHer co-stained boutons. Average normalized (norm.) fluorescence responses to 50 action potentials at 20 Hz (n = 3 experiments with >50 boutons for each). The spH fluorescence (black) shows little or no recovery, whereas the cypHer signal (gray) shows normal fluorescence recovery, demonstrating that the Syt1 molecules that were endocytosed constitute a different population from those freshly exocytosed. Error bars represent s.e.m. (**b**,**c**) Photobleaching for 5 min at external pH 8.5 preferentially affects the vesicular pool of cypHer-tagged molecules. Fifty action potentials at 20 Hz induced typical spH fluorescence transients (black, n = 5 experiments with >50 boutons for each). However, the cypHer signal (gray) for both Syt1 (**b**) and VGAT (**c**) increases in parallel to the spH decay, indicating endocytosis of vesicle proteins from an RRetP resident on the bouton membrane. Error bars represent s.e.m. (**d**,**e**) Average fluorescence profiles of boutons (n = 3 experiments with >50 boutons for each) labeled with only anti-Syt1–cypHer (**d**) or anti-VGAT–cypHer (**e**). Experiments were performed as in panels **b** and **c**, but using non-transfected neuronal cultures. This indicates that spH overexpression does not alter the dynamics or size of the RRetP. Error bars represent s.e.m. (**f**) Comparison of RRP and RRetP sizes measured by different labeling strategies for Syt1 and VGAT. 'Prebleach' denotes the cypHer fluorescence decrease upon 50 action potentials at 20 Hz, a measure of the RRP size (40.2 ± 6.9 a.u. for Syt1 and 34.8 ± 3. 6 a.u. for VGAT). 'Postbleach' denotes the fluorescence increase (19.5 ± 6.2 a.u. for Syt1 and 17.7 ± 2.1 a.u. for VGAT) subsequent to vesicular cypHer bleaching upon 50 action potentials at 20 Hz (as shown in **d** and **e**). 'Surface staining' denotes the fluorescence increase upon 50 action potentials at 20 Hz (53. 7 ± 4.8 a.u.) after preferential labeling of the Syt1 surface pool (see **Fig. 5a**). Error bars represent s.e.m.

actively participate in endocytic recycling, implying that vesicles being exo- and endocytosed by the same stimulus consist of different individual molecules[11,13]. However, it has not been possible so far to directly study the kinetics of this functional surface pool with an optical tracer that selectively labels the native proteins. By engineering a tobacco etch virus (TEV) cleavage site between the vesicle protein Syb2 and pHluorin, however, the fluorescence of surface spH could be eliminated by TEV digestion and its participation in recycling could be shown indirectly[13]. Thus, we labeled spH-TEV transfected neurons with anti-Syt1–cypHer or anti-VGAT–cypHer and incubated them with TEV protease for 15 min[13] to silence the non-vesicular surface spH-TEV fluorescence while keeping anti-Syt1–cypHer unperturbed. Next, we elicited 50 action potentials at 20 Hz, a stimulus that was shown to deplete the RRP of docked vesicles in hippocampal boutons[31,32]. An increase in fluorescence was observed in the spH trace followed by little or no recovery (**Fig. 4a**, top), indicating that instead of freshly exocytosed synaptic vesicle constituents, cleaved surface spH-TEV was preferentially retrieved[13]. Is this preferential uptake of membrane spH a mere overexpression artifact due to surface-stranded spH? Or does it represent a specific retrieval mechanism? The fluorescence transient in the simultaneously recorded cypHer channel, which labels endogenous Syt1 in the same synaptic vesicles, showed unperturbed fluorescence recovery, suggesting that endocytosis and reacidification of synaptic vesicles were normal (**Fig. 4a**, bottom). This shows that synaptic vesicle proteins are endocytosed but are derived from a functional surface pool[13,34].

Using spH-TEV, however, we were not able to directly visualize and prove the retrieval from the surface pool. Now, using cypHer, which has a pH dependence that is opposite to that of spH, we could perform the reverse experiment. We selectively silenced most of the vesicular cypHer fluorescence in spH-transfected boutons by photobleaching at 640 nm for 5 min. To minimize photobleaching of surface anti-Syt1–cypHer, we transiently bathed neurons in extracellular buffer of pH 8.5. Stimulation with 50 action potentials at 20 Hz induced typical spH fluorescence transients (**Fig. 4b**, top), but prebleaching the vesicle pool abolished most of the exocytic fluorescence decrease of the cypHer signal during stimulation (**Fig. 4b**, bottom). Notably, after stimulation onset, the cypHer fluorescence increases and reaches a plateau, which demonstrates the retrieval of non-bleached cypHer-labeled Syt1 molecules from the presynaptic membrane. This reaffirms the existence of an RRetP of presorted synaptic vesicle constituents on the presynaptic membrane that are preferentially endocytosed on exocytosis, a pool we previously termed an 'easily retrievable pool'[3]. A slight delay or even small downward dip in the cypHer traces is fully explained by incomplete bleaching of the vesicular fluorescence, which results in some remaining contribution of exocytosis. Even at pH 8.5 the cypHer surface fluorescence is reduced less than 90%, so it would be substantially bleached when attempting to fully bleach the vesicular fraction by using longer bleaching times. Next, we tested whether such a RRetP also exists for other synaptic vesicle proteins, such as VGAT, which is expected to be present only in very low copy numbers in synaptic vesicles[35]. We repeated the same experiment using spH-transfected neurons co-stained with anti-VGAT–cypHer (**Fig. 4c**), revealing that even for low-copy-number synaptic vesicle proteins, there exists a surface pool that is preferentially recycled by the endocytic machinery.

To rule out the possibility that spH overexpression might have altered the targeting of synaptic vesicle proteins to the vesicular and surface pools, we repeated the above experiments using only

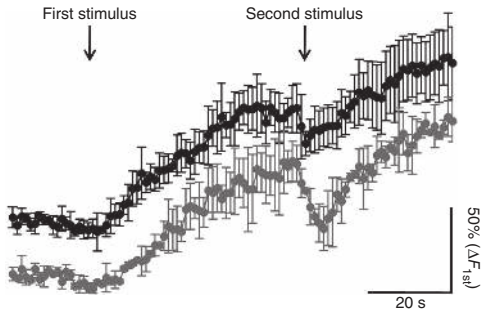

Figure 5 Repeated stimulation reveals reuse of the RRetP. Average fluorescence profile of surface Syt1-labeled boutons ($n = 3$ experiments with >50 boutons for each) stimulated first with 50 action potentials at 20 Hz followed by a second stimulation with either 50 (black) or 200 (gray) action potentials at 20 Hz (gray). In response to the second stimulus, a marked fraction of synaptic vesicles recycled from the RRetP upon the first stimulus is released. Error bars represent s.e.m.

exogenous cypHer reporters (**Fig. 4d**,**e**). Both the kinetics and amplitude of cypHer transients were comparable to those determined by the dual-color recordings, showing that compensatory endocytosis of Syt1 or VGAT is not perturbed by spH overexpression and primarily draws upon a functional pool of synaptic vesicle constituents on the presynaptic membrane.

We next compared the size of the RRP—that is, the fluorescence drop on 50 action potentials (**Fig. 4a**, bottom)—to that of the RRetP—that is, the cypHer fluorescence increase on 50 action potentials after vesicular cypHer bleaching (**Fig. 4d**,**e**). The estimated mean size of the RRP was 40.2 ± 6.9 a.u. for anti-Syt1–cypHer and 34.8 ± 3.6 a.u. for anti-VGAT–cypHer (**Fig. 4f**), whereas the mean RRetP size turned out to be only 19.5 ± 6.2 a.u. for anti-Syt1–cypHer and 17.7 ± 2.1 a.u. for anti-VGAT–cypHer. These smaller size estimates of the RRetP might be solely attributed to partial bleaching of the surface pool. Thus, to avoid prebleaching, we attempted to preferentially stain the surface Syt1 pool (compare with **Fig. 2c**). Neurons were briefly incubated with a saturating concentration of anti-Syt1–cypHer in the presence of tetrodotoxin (TTX) for 5 min. Again, when stimulated with 50 action potentials at 20 Hz (**Fig. 5**), the fluorescence signal increased to a plateau as in the vesicular cypHer bleaching experiments. The fluorescence increase, which is a measure of the RRetP, was 53.7 ± 4.8 a.u. (**Fig. 4f**), which is similar to the measured RRP size (**Fig. 4a**). Thus, the RRP seems to be counterbalanced by an RRetP of similar size.

Can synaptic vesicle recycled from the RRetP be re-released on repeated stimulation? To answer this question, a second bout of stimulation to surface Syt1-labeled boutons was applied 60 s later (**Fig. 5**). The cypHer fluorescence responses indeed now showed a fast drop owing to partial exocytosis of previously recycled RRetP components followed by an increase indicating endocytosis. Released fractions were 27.6 ± 5.1% for 50 action potentials and 49.7 ± 9.2% for 200 action potentials, which is in close agreement with similar experiments using FM styryl dyes as tracers[36]. However, unexpectedly, the endocytic increases for the second stimulus clearly exceeded the exocytic drops. This could be due to incomplete depletion of the RRetP during the first stimulus of 50 action potentials (compare with

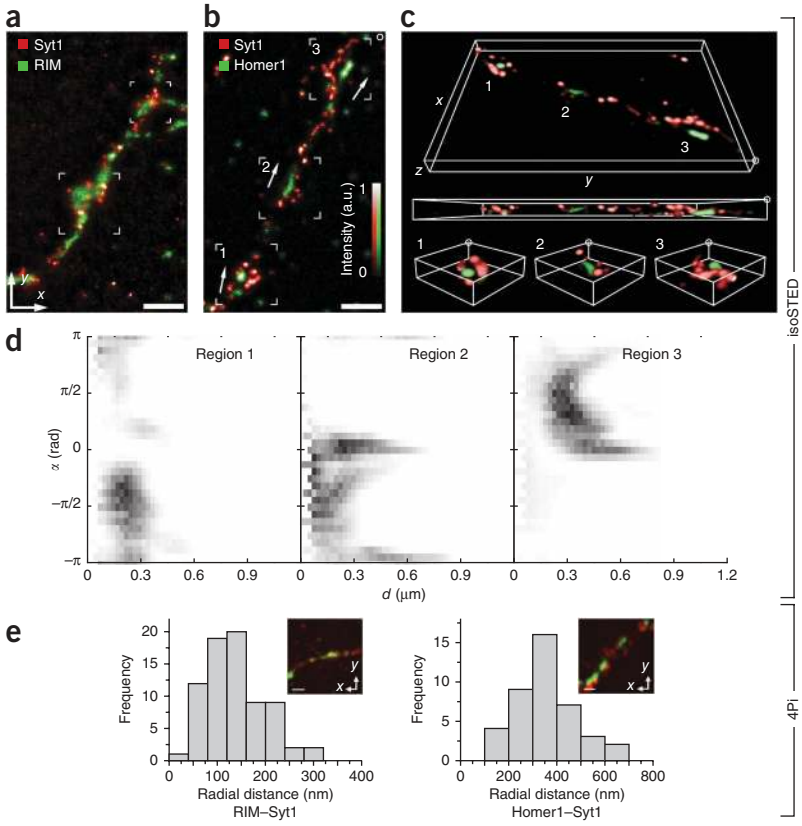

Figure 6 Spatial organization of the RRetP. Three-dimensional dual-color isoSTED nanoscopy of cultured hippocampal boutons showing the localization of surface-stranded Syt1 (red) at synapses identified by the pre- and postsynaptic markers RIM1 and RIM2 (RIM) and Homer1 (green), supported by 4Pi microscopy data of a large number of synapses. (**a**) *z*-projection of a three-dimensional image stack of Syt1 at synapses labeled by the CAZ markers RIM1 and RIM2. (**b**) *z*-projection as in **a** of Syt1 at synapses labeled by Homer1 as a PSD marker, with synapses at regions of interest numbered 1 to 3. Arrows mark the local orientation of the axon. (**c**) Perspective views of volume-rendered data. The Syt1 labeling reveals preassembled patches that are localized in the periphery of the active zone, typically within 500 nm distance from the postsynaptic marker. (**d**) Spatial distribution of Syt1 with respect to Homer1 for each region of interest. Histograms show Syt1–Homer1 cross-correlation, binned according to Syt1–Homer1 distance d and relative azimuth angle α, which was measured with respect to the orientation of the axon as marked by arrows in **b**. Distances between Syt1 patches and the postsynaptic marker accumulate at about 100–300 nm at angles where the probability of finding Syt1 patches that are not associated with Homer1 is reduced (α deviating from 0 and ± π). (**e**) Nearest neighbor distances between Syt1 and RIM1 and RIM2 (RIM) or Homer1 patches from dual-color 4Pi microscopy stacks of $n = 74$ (RIM1 and RIM2) and $n = 41$ (Homer1) synapses. Insets show examples of *z*-projections. Scale bars represent 1 μm. Rendering volumes: 4.5 μm × 7.0 μm × 0.4 μm for the full data set; 1.5 μm × 1.5 μm × 0.4 μm for regions of interest.

Supplementary Fig. 3), but is more likely to be due to partial replenishment of the RRetP after the first stimulus by exocytosed vesicles that had taken up cypHer by spontaneous recycling during the initial labeling phase.

Spatial organization of the RRetP

How is the functional surface pool spatially organized at the presynapse? To address this, we used the same antibody, anti-Syt1, to specifically label the surface pool. After labeling at 4 °C, we fixed the cells immediately and identified synapses by colabeling with antibodies to bona fide CAZ or PSD proteins. The spatial organization of the Syt1 surface pool was investigated using dual-color isoSTED[24] nanoscopy. In the three-dimensional reconstruction of hippocampal *en passant* boutons from isoSTED image stacks (**Fig. 6a–c**), we found distinct Syt1 patches in the vicinity of the active zones.

From a large list of antibodies to CAZ elements, we obtained good signal-to-noise ratio only for antibodies to RIM1 and RIM2. The observed antibody fluorescence distribution was broad (**Fig. 6a**), extending up to 1 µm along its long axis. Although large active-zone sizes of up to 700 nm have been documented in hippocampal synapses in electron microscopy of single sections[33], as well as in recent full three-dimensional reconstructions[37], the even larger patches seen in our experiment indicate that active-zone sizes are indeed overestimated by labeling the large RIM proteins at the N-terminal zinc-finger domain.

To provide an additional fingerprint of synapses, we modified our staining by targeting the PSD opposing the active zone with antibodies to Homer1. This introduced a characteristic spatial separation between the two channels (**Fig. 6b**). We analyzed the distribution of the Syt1 patches with respect to Homer1 in each of the three bouton regions (**Fig. 6c**), as depicted in the histograms (**Fig. 6d**). Mean distances between Syt1 and Homer1 increase as the azimuth angle α between the estimated orientation of the axon (**Fig. 6b**, arrows) and the Syt1–Homer1 connecting vectors approaches 0 or $\pm\pi$, owing to a higher probability of including Syt1 patches that are localized adjacent on the axolemma but that are not associated with Homer1. At other angles, the observed distances are smaller and reach minimum distances of about 100–300 nm for a bouton (**Fig. 6d**). This finding agrees well with a localization analysis of a large number of synapses in 4Pi microscopy[22,23] image stacks (**Fig. 6e** and **Supplementary Fig. 4**). Considering this result together with our live cell imaging data, we therefore suggest that the associated Syt1 patches constitute the preassembled RRetP.

DISCUSSION

We have devised a new technique to measure stimulation-dependent exo-endocytosis in hippocampal presynaptic boutons. Using cypHer-conjugated antibodies to Syt1 and VGAT, we achieved specific labeling of endogenous vesicle proteins. However, antibody uptake into synaptic vesicles during the 3–4 h incubation at 37 °C might be mediated to a large degree by spontaneous recycling, and thus might label a different synaptic vesicle pool in comparison to stimulation-induced uptake[38–40]. But analysis of spontaneous and evoked recycling using anti-Syt1-cypHer revealed that both modes of release draw on a common pool of synaptic vesicles at these central synapses[41]. The good spectral separation between cypHer and spH allowed us to use the two pH-dependent optical reporters in tandem, resulting in two independent readouts of presynaptic activity. Action potential–driven fluorescence transients of anti-Syt1–cypHer and anti-VGAT–cypHer-stained boutons show transients that were the mirror image of spH transients owing to their opposite pH dependence of cypHer fluorescence. However, kinetics of endocytosis and reacidification assayed by both methods were nearly identical, showing that this cypHer-based approach reliably monitors recycling of endogenous synaptic vesicle proteins.

By fluorescently silencing the surface spH, we could clearly demonstrate that the vesicle proteins exo- and endocytosed were not the same individual molecules, as previously shown[13]. But the unaffected cypHer fluorescence transient enabled us for the first time, to our knowledge, to monitor the endocytosis of RRetP-derived synaptic vesicles that contain cleaved spH and endogenous Syt1 labeled with anti-Syt1–cypHer. To provide direct evidence that this surface pool actively participates in exo-endocytosis, we photobleached the vesicular cypHer signal from anti-Syt1–cypHer and anti-VGAT–cypHer stained boutons and elicited 50 action potentials, a stimulus that has been previously shown to deplete the RRP. The observed increase in cypHer fluorescence, in parallel to the spH fluorescence decay, demonstrates preferential endocytosis of cypHer-stained Syt1 and VGAT residing on the bouton membrane. This preferential recruitment of surface synaptic vesicle proteins on stimulation was not affected by spH overexpression, thus validating our and others' previous pHluorin-based results[11,13]. Although overexpression of some pHluorin fusion proteins leads to an excess of surface-stranded proteins, it has been shown to not affect the functional size of this pool[11,13]. The size of this RRetP could be determined by selective dequenching of surface-bound anti-Syt1–cypHer with brief pulses of acidic buffer. We found that retrieval from the RRetP could counterbalance exocytosis for up to 70 action potentials at 20 Hz. We further measured the size of this functional surface pool by preferentially staining surface Syt1 and monitoring its endocytosis, which yielded comparable estimates. Thus, the RRetP has a capacity similar to the RRP. This is also corroborated by the nanoscopy of surface-stranded Syt1 at the periactive zone, which is generally identified as the site of endocytosis[14,15,25,42]; this revealed several preassembled patches, from which new synaptic vesicles could bud. Moreover, we note that even for the low-copy-number protein VGAT, there was a functional surface pool that was preferentially internalized upon stimulated exo-endocytosis, raising the question of whether this transporter could be active in the plasma membrane.

Our findings demonstrate the existence of a functional RRetP of native vesicle constituents such as Syt1 and VGAT at the periactive zone. The preferential uptake of vesicle constituents from a surface pool explains why synaptic vesicles exo- and endocytosed do not consist of identical individual molecules. Although overexpression of spH may lead to a substantial increase of the total surface pool, the cypHer experiments clearly show the existence of an endogenous synaptic vesicle protein surface pool participating in synaptic vesicle recycling. Existence of an RRetP can explain the first wave of clathrin-mediated endocytosis observed in the first reconstruction of the endocytic time course from electron micrographs of frog neuromuscular junctions[18]. Also, it can explain why the initial endocytic rate remains constant irrespective of the stimulation strength, as suggested in other studies[29,30]. However, after this RRetP is depleted at ~70 action potentials, the rate drops because the endocytic machinery has to invest more energy and time to recapture and re-sort freshly exocytosed components to the sites of retrieval. Because endocytosis of the RRetP (**Fig. 4**) itself , however, takes several seconds, the main advantage of an RRetP might not be so much a gain in speed but rather a gain in precision of re-sorting and reclustering to ensure maximum fusion competence of newly endocytosed vesicles. This is in line with the counterintuitive finding that knockdown or knockout of major sorting factors such as activator protein 1 (AP1) and AP2 subunits results in similar or even faster endocytic kinetics of a large fraction of retrieved synaptic vesicle proteins[43,44], probably corresponding to

bulk endocytosis. However, the re-availability of endocytosed synaptic vesicles is slowed and their fusion competence is diminished[44].

In three recent studies, the importance of Ca^{2+} for coupling of exo- and endocytosis is emphasized[45–47]. Work in *D. melanogaster* suggests that there might be a vesicular Ca^{2+} channel that, once incorporated into the plasma membrane by fusion, would allow Ca^{2+} entry at the site of endocytosis and thus might trigger the retrieval from the RRetP[47]. However, the detailed molecular mechanism that couples exocytosis from the RRP with compensatory endocytosis from the RRetP remains to be elucidated.

METHODS

Methods and any associated references are available in the online version of the paper at http://www.nature.com/natureneuroscience/.

Note: Supplementary information is available on the Nature Neuroscience website.

ACKNOWLEDGMENTS

We thank M. Pilot and I. Herfort for the preparation of primary cell cultures of hippocampal neurons and E. Neher and R.H. Chow for critical reading of the manuscript. We acknowledge D. Boening and M. Martineau for experimental support and we are grateful to K. Kolmakov and V. Belov (Max Planck Institute for Biophysical Chemistry, Goettingen) for providing us with the new fluorescent dye KK114. We thank G. Miesenböck (Oxford University) for providing superecliptic spH. We would also like to thank M. Hoon and N. Glyvuk for suggestions. This work was supported by grants from the European Science Foundation/Deutsche Forschungsgemeinschaft (DFG) (EUROMEMBRANE programme, EuroSynapse CRP FP-020 to J.K.) as well as from the DFG (Kl 1334/1-1 to C.S.T. and J.K., SFB 944 to J.K., CMPB to A.E. and S.W.H., and SFB755 to A.E. and S.W.H.). Y.H. is supported by a stipend from the Max-Planck Foundation and R. Sinha is supported by a stipend from the International Max Planck Research School in Neurosciences at the University of Goettingen.

AUTHOR CONTRIBUTIONS

Y.H., R. Sinha and C.S.T. conducted the majority of the experiments. J.H. collected and analyzed the 4Pi microscopy data. IsoSTED microscopy and analysis was performed by R. Schmidt and A.E. in the department of S.W.H. H.M. synthesized the cypHer-conjugated antibodies. J.K. conceptualized the project and together with Y.H. and R. Sinha designed the experiments. R. Sinha and J.K. wrote the paper with the help of Y.H., C.S.T. and R. Schmidt. All authors discussed the results and commented on the manuscript.

COMPETING FINANCIAL INTERESTS

The authors declare no competing financial interests.

Published online at http://www.nature.com/natureneuroscience/.
Reprints and permissions information is available online at http://www.nature.com/reprints/index.html.

1. Heuser, J.E. & Reese, T.S. Evidence for recycling of synaptic vesicle membrane during transmitter release at the frog neuromuscular junction. *J. Cell Biol.* **57**, 315–344 (1973).
2. Granseth, B., Odermatt, B., Royle, S.J. & Lagnado, L. Clathrin-mediated endocytosis is the dominant mechanism of vesicle retrieval at hippocampal synapses. *Neuron* **51**, 773–786 (2006).
3. Mueller, V.J., Wienisch, M., Nehring, R.B. & Klingauf, J. Monitoring clathrin-mediated endocytosis during synaptic activity. *J. Neurosci.* **24**, 2004–2012 (2004).
4. Wu, L.G., Ryan, T.A. & Lagnado, L. Modes of vesicle retrieval at ribbon synapses, calyx-type synapses, and small central synapses. *J. Neurosci.* **27**, 11793–11802 (2007).
5. He, L., Wu, X.S., Mohan, R. & Wu, L.G. Two modes of fusion pore opening revealed by cell-attached recordings at a synapse. *Nature* **444**, 102–105 (2006).
6. Zhang, Q., Li, Y. & Tsien, R.W. The dynamic control of kiss-and-run and vesicular reuse probed with single nanoparticles. *Science* **323**, 1448–1453 (2009).
7. Ceccarelli, B., Hurlbut, W.P. & Mauro, A. Turnover of transmitter and synaptic vesicles at the frog neuromuscular junction. *J. Cell Biol.* **57**, 499–524 (1973).
8. Gandhi, S.P. & Stevens, C.F. Three modes of synaptic vesicular recycling revealed by single-vesicle imaging. *Nature* **423**, 607–613 (2003).
9. Koenig, J.H., Yamaoka, K. & Ikeda, K. Omega images at the active zone may be endocytotic rather than exocytotic: implications for the vesicle hypothesis of transmitter release. *Proc. Natl. Acad. Sci. USA* **95**, 12677–12682 (1998).
10. Miesenböck, G., De Angelis, D.A. & Rothman, J.E. Visualizing secretion and synaptic transmission with pH-sensitive green fluorescent proteins. *Nature* **394**, 192–195 (1998).
11. Fernández-Alfonso, T., Kwan, R. & Ryan, T.A. Synaptic vesicles interchange their membrane proteins with a large surface reservoir during recycling. *Neuron* **51**, 179–186 (2006).
12. Dittman, J.S. & Kaplan, J.M. Factors regulating the abundance and localization of synaptobrevin in the plasma membrane. *Proc. Natl. Acad. Sci. USA* **103**, 11399–11404 (2006).
13. Wienisch, M. & Klingauf, J. Vesicular proteins exocytosed and subsequently retrieved by compensatory endocytosis are nonidentical. *Nat. Neurosci.* **9**, 1019–1027 (2006).
14. Teng, H., Cole, J.C., Roberts, R.L. & Wilkinson, R.S. Endocytic active zones: hot spots for endocytosis in vertebrate neuromuscular terminals. *J. Neurosci.* **19**, 4855–4866 (1999).
15. Teng, H. & Wilkinson, R.S. Clathrin-mediated endocytosis near active zones in snake motor boutons. *J. Neurosci.* **20**, 7986–7993 (2000).
16. Taubenblatt, P., Dedieu, J.C., Gulik-Krzywicki, T. & Morel, N. VAMP (synaptobrevin) is present in the plasma membrane of nerve terminals. *J. Cell Sci.* **112**, 3559–3567 (1999).
17. Willig, K.I., Rizzoli, S.O., Westphal, V., Jahn, R. & Hell, S.W. STED microscopy reveals that synaptotagmin remains clustered after synaptic vesicle exocytosis. *Nature* **440**, 935–939 (2006).
18. Miller, T.M. & Heuser, J.E. Endocytosis of synaptic vesicle membrane at the frog neuromuscular junction. *J. Cell Biol.* **98**, 685–698 (1984).
19. Balaji, J. & Ryan, T.A. Single-vesicle imaging reveals that synaptic vesicle exocytosis and endocytosis are coupled by a single stochastic mode. *Proc. Natl. Acad. Sci. USA* **104**, 20576–20581 (2007).
20. Adie, E.J. *et al.* CypHer 5: a generic approach for measuring the activation and trafficking of G protein-coupled receptors in live cells. *Assay Drug Dev. Technol.* **1**, 251–259 (2003).
21. Martens, H. *et al.* Unique luminal localization of VGAT-C terminus allows for selective labeling of active cortical GABAergic synapses. *J. Neurosci.* **28**, 13125–13131 (2008).
22. Hüve, J., Wesselmann, R., Kahms, M. & Peters, R. 4Pi microscopy of the nuclear pore complex. *Biophys. J.* **95**, 877–885 (2008).
23. Kano, H., Jakobs, S., Nagorni, M. & Hell, S.W. Dual-color 4Pi-confocal microscopy with 3D-resolution in the 100 nm range. *Ultramicroscopy* **90**, 207–213 (2001).
24. Schmidt, R. *et al.* Spherical nanosized focal spot unravels the interior of cells. *Nat. Methods* **5**, 539–544 (2008).
25. Roos, J. & Kelly, R.B. The endocytic machinery in nerve terminals surrounds sites of exocytosis. *Curr. Biol.* **9**, 1411–1414 (1999).
26. Shupliakov, O. *et al.* Impaired recycling of synaptic vesicles after acute perturbation of the presynaptic actin cytoskeleton. *Proc. Natl. Acad. Sci. USA* **99**, 14476–14481 (2002).
27. Gundelfinger, E.D., Kessels, M.M. & Qualmann, B. Temporal and spatial coordination of exocytosis and endocytosis. *Nat. Rev. Mol. Cell Biol.* **4**, 127–139 (2003).
28. Sankaranarayanan, S., De Angelis, D., Rothman, J.E. & Ryan, T.A. The use of pHluorins for optical measurements of presynaptic activity. *Biophys. J.* **79**, 2199–2208 (2000).
29. Sankaranarayanan, S. & Ryan, T.A. Real-time measurements of vesicle-SNARE recycling in synapses of the central nervous system. *Nat. Cell Biol.* **2**, 197–204 (2000).
30. Fernández-Alfonso, T. & Ryan, T.A. The kinetics of synaptic vesicle pool depletion at CNS synaptic terminals. *Neuron* **41**, 943–953 (2004).
31. Schikorski, T. & Stevens, C.F. Quantitative ultrastructural analysis of hippocampal excitatory synapses. *J. Neurosci.* **17**, 5858–5867 (1997).
32. Murthy, V.N. & Stevens, C.F. Reversal of synaptic vesicle docking at central synapses. *Nat. Neurosci.* **2**, 503–507 (1999).
33. Schikorski, T. & Stevens, C.F. Morphological correlates of functionally defined synaptic vesicle populations. *Nat. Neurosci.* **4**, 391–395 (2001).
34. Tabares, L. *et al.* Monitoring synaptic function at the neuromuscular junction of a mouse expressing synaptopHluorin. *J. Neurosci.* **27**, 5422–5430 (2007).
35. Takamori, S. *et al.* Molecular anatomy of a trafficking organelle. *Cell* **127**, 831–846 (2006).
36. Vanden Berghe, P. & Klingauf, J. Synaptic vesicles in rat hippocampal boutons recycle to different pools in a use-dependent fashion. *J. Physiol. (Lond.)* **572**, 707–720 (2006).
37. Staras, K. *et al.* A vesicle superpool spans multiple presynaptic terminals in hippocampal neurons. *Neuron* **66**, 37–44 (2010).
38. Fredj, N.B. & Burrone, J. A resting pool of vesicles is responsible for spontaneous vesicle fusion at the synapse. *Nat. Neurosci.* **12**, 751–758 (2009).
39. Groemer, T.W. & Klingauf, J. Synaptic vesicles recycling spontaneously and during activity belong to the same vesicle pool. *Nat. Neurosci.* **10**, 145–147 (2007).
40. Sara, Y., Virmani, T., Deak, F., Liu, X. & Kavalali, E.T. An isolated pool of vesicles recycles at rest and drives spontaneous neurotransmission. *Neuron* **45**, 563–573 (2005).
41. Hua, Y., Sinha, R., Martineau, M., Kahms, M. & Klingauf, J. A common origin of synaptic vesicles undergoing evoked and spontaneous fusion. *Nat. Neurosci.* **13**, 1451–1453 (2010).
42. Brodin, L. & Shupliakov, O. Giant reticulospinal synapse in lamprey: molecular links between active and periactive zones. *Cell Tissue Res.* **326**, 301–310 (2006).
43. Kim, S.H. & Ryan, T.A. Synaptic vesicle recycling at CNS synapses without AP-2. *J. Neurosci.* **29**, 3865–3874 (2009).
44. Glyvuk, N. *et al.* AP-1/σ1B-adaptin mediates endosomal synaptic vesicle recycling, learning and memory. *EMBO J.* **29**, 1318–1330 (2010).
45. Hosoi, N., Holt, M. & Sakaba, T. Calcium dependence of exo- and endocytotic coupling at a glutamatergic synapse. *Neuron* **63**, 216–229 (2009).
46. Wu, X.S. *et al.* Ca^{2+} and calmodulin initiate all forms of endocytosis during depolarization at a nerve terminal. *Nat. Neurosci.* **12**, 1003–1010 (2009).
47. Yao, C.K. *et al.* A synaptic vesicle-associated Ca^{2+} channel promotes endocytosis and couples exocytosis to endocytosis. *Cell* **138**, 947–960 (2009).

ONLINE METHODS

Cell culture. Primary cultures of rat hippocampal neurons were prepared from the CA3-CA1 region of 1- or 2-day-old Wistar rats and transfected with super-recliptic spH at 3 d *in vitro* by a modified calcium phosphate transfection procedure[13]. For super-resolution microscopy, Banker-type cultures of rat hippocampal neurons from 1- to 3-day-old Wistar rats were prepared and seeded on glass coverslips[48]. All imaging experiments were carried out at 14–21 d *in vitro*.

TEV protease cleavage. Neurons transfected with spH-TEV were incubated with AcTEV protease and 1 mM dithiothreitol (Invitrogen) for 15 min at 20–25 °C, as described previously[13]. After digestion, neurons were washed several times with normal Tyrode solution to remove the enzyme. Cleavage of the surface spH was observed over time as a reduction in the fluorescence signal.

Immunostaining. Two cypHer-conjugated antibodies, anti-Syt1–cypHer and anti-VGAT–cypHer, were used to label hippocampal neurons. Neurons were incubated with either anti-Syt1–cypHer or anti-VGAT–cypHer at 37 °C for 3–4 h in a carbonate buffer containing 120 mM NaCl, 5 mM KCl, 1 mM $MgCl_2$, 2.5 mM $CaCl_2$, 10 mM glucose and 18 mM $NaHCO_3$ at pH ~7.4. The cells were then washed twice and placed in a perfusion chamber containing modified Tyrode solution (150 mM NaCl, 4 mM KCl, 1 mM $MgCl_2$, 2 mM $CaCl_2$, 10 mM glucose and 10 mM HEPES buffer at pH ~7.4). Acidic buffer with final pH of 5.5 and 6.5 was prepared by replacing HEPES with 2-(*N*-morpholino)ethanesulfonic acid (MES), whereas alkaline solution with pH 8.5 and 9.5 was prepared by replacing HEPES with *N*,*N*-bis-(2-hydroxyethyl)glycine (BICIN). All other components remained unchanged.

For pH titration measurements of cypHer, anti-Syt1–cypHer-labeled neurons were stained, washed and then fixed with 4% (wt/vol) paraformaldehyde (PFA). Cells were permeabilized with 0.4% (wt/vol) saponin to make the internalized antibodies accessible to perfusion with buffers of differing pH. The surface pool stainings for **Figures 4f** and **5** were performed by incubating the neurons with saturating concentrations of anti-Syt1–cypHer in the presence of 0.5 µm TTX for 5 min at 20–25 °C. The neurons were then washed with normal Tyrode solution and used for imaging.

To label the surface fraction of Syt1 for super-resolution microscopy, live hippocampal neurons on coverslips were washed three times in Ca^{2+}-free solution (120 mM NaCl, 5 mM KCl, 3.5 mM $MgCl_2$, 10 mM D-glucose, 10 mM HEPES and 1 mM EGTA) containing 0.5 µM TTX and incubated with the Syt1 mouse monoclonal antibody (604.1; 1:10 cell culture supernatant; Synaptic Systems) and 2% (vol/vol) goat serum for 45 min at 4 °C. After three wash steps, cells were fixed for 10 min at 20–25 °C in 4% PFA and washed again four times for 3 min. For labeling of Homer1 or RIM1 and RIM2, cells were permeabilized and simultaneously blocked with buffer containing 2% goat serum, 1% (wt/vol) BSA and 0.4% saponin for 15 min. Subsequently, coverslips were incubated for 1 h at 20–25 °C with a rabbit polyclonal antibody to Homer1 or to the RIM1 and RIM2 zinc-finger domains (1:100; Synaptic Systems) using the same buffer conditions as for blocking. After washing four times for 3 min, secondary antibodies labeled with KK114 (1:100) and DY-480XL (1:100, Dyomics GmbH) were applied for isoSTED imaging, whereas secondary antibodies labeled with Alexa 488 (1:100; Invitrogen) and Alexa 594 (1:100; Invitrogen) were applied for 4Pi microscopy The secondary antibodies were incubated for 1 h at 20–25 °C. After four final wash steps for 3 min, the coverslips were mounted and used for isoSTED imaging or 4Pi microscopy.

Epifluorescence microscopy. Synaptic boutons were stimulated by electric field stimulation using platinum electrodes spaced at 10 mm with 1 ms pulses of 50 mA and alternating polarity applied by a constant current stimulus isolator (WPI A 385, World Precision Instruments); 10 mM 6-cyano-7-nitroquinoxaline-2,3-dione (CNQX) and 50 mM D,L-2-amino-5-phosphonovaleric acid (AP5) were added to prevent recurrent activity. Fast solution exchanges were achieved through a two-barrel glass tubing perfusion system controlled by a piezo-controlled stepper device (SF778, Warner Instruments).

Image acquisition for experiments in **Figures 1c–f**, **2** and **3** and **Supplementary Figure 1** were performed at 20–25 °C by a cooled, slow-scan CCD camera (SensiCam-QE, PCO) mounted on an inverted microscope (Axiovert S100TV, Zeiss) with a ×63, 1.2 numerical aperture water-immersion objective and an FITC/Cy5 dual-band filter set (AHF analysentechnik AG). SpH and cypHer were excited at 480 nm and 640 nm, respectively, with a computer-controlled monochromator (Polychrom II, Till Photonics). Time lapse images of spH (green) and cypHer (red) were acquired alternating between the channels at 0.5 Hz. For RRetP visualization experiments in **Figures 4** and **5**, an electron-multiplying CCD (Andor iXon+ DU-897E-BV camera; Andor Technology) controlled by Andor iQ Software (Andor Technology) was mounted on an inverted Nikon TE2000 microscope equipped with a ×60, 1.2 numerical aperture water-immersion objective and an FITC/Cy5 dual-band filter set (AHF analysentechnik AG). Vesicular cypHer was photobleached by continuous exposure to red light (640 nm) for 5 min. During the cypHer bleaching procedure, cells were bathed in an alkaline buffer solution of pH 8.5 for better protection of surface-bound cypHer molecules.

Images were analyzed using self-written routines in Matlab (MathWorks). Active boutons were localized on the basis of spH fluorescence using an automated routine in which a difference image is generated by subtracting an average of five frames before from after stimulation. Spots on the difference image, each representing a putative functional bouton, were identified and centered on the basis of the maximum pixel intensity. Only spots with fluorescence response >2σ of baseline fluorescence were chosen for analysis. Square regions of interest (1.5 × 1.5 μm^2) were centered on these spots in both the spH and cypHer channel and average fluorescence profiles were then plotted. Owing to the low transfection efficiency of spH, not every cypHer-positive bouton was spH positive. For dual-color recordings, we used the coordinates of the regions of interest identified from spH response to define the positions of active boutons in the cypHer channel. Fluorescence traces from individual boutons were normalized before calculating the average response.

As the cypHer fluorophore is much less photo-stable than its prototype (cyanine 5 dye), in some of the initial experiments (**Figs. 1c–f**, **2a**,**b** and **3** and **Supplementary Fig. 1**) in which an electron-multiplying CCD was not used the intensity of time-lapse images was corrected for photobleaching. By taking into account that cypHer molecules would be quenched and temporarily protected from photobleaching upon exocytosis, the kinetics of exo-endocytosis could be successfully isolated using an iterative deconvolution algorithm. The intensity decline due to photobleaching can be described as an exponential decay (see below), where $I(t)$ is the instantaneous intensity. The decay constant λ can be obtained from time-lapse image series with similar image acquisition settings as in experiments but in absence of stimulation:

$$\frac{dI(t)}{dt} = -\lambda I(t)$$

Therefore, the instantaneous change in fluorescence $\Delta I(t)$ caused by exo-endocytosis can be determined iteratively by the following equation, where $I(0)$ is the instantaneous intensity observed at time 0. An example of the correction is shown in **Supplementary Figure 1**.

$$I(t) = I(0) - \sum_{i=0}^{t-1} \lambda I(i) + \Delta I(t)$$

4Pi microscopy. Cells were covered with 20 µl of buffer (see "Immunostaining") and sealed by a second coverslip with immobilized red fluorescent beads (TransFluoSpheres: NeutrAvidin-labeled microspheres (Invitrogen), 0.1 µm, excitation maximum 488 nm; emission maximum 605 nm), resulting in a space between the two coverslips of less than 30 µm.

Images were obtained with a commercial 4Pi microscope (TCS 4Pi microscope type A, Leica Microsystems) employing water immersion lenses (×63, numerical aperture 1.2) and oil immersion lenses (×100, numerical aperture 1.46). For two-photon excitation, a mode-locked titanium:sapphire laser (Mai Tai, Spectra Physics GmbH) with pulse length stretched to >1 ps was used. The laser was tuned by a grating to a wavelength between 770 and 820 nm. The beam expander was set to 3 or 6. Fluorescence originating from the sample was passed through a filter cube (short-pass 700 nm, beam splitter 560 nm, band-pass 500–550 nm, and band-pass 607–683 nm), and its intensity was measured by photon-counting avalanche photodiodes (PerkinElmer). The detection pinhole was set to 0.86 Airy units. Samples were mounted between the two objectives, and focus and phase of the counterpropagating beams were prealigned to the immobilized beads. Then stacks of the cells were recorded with a pixel size between 10 × 10 nm^2

doi:10.1038/nn.2838

and 18 × 18 nm^2 in the *x*–*z* direction. The step size in the *y* direction was 97 nm with water immersion lenses and 61 nm with oil immersion lenses.

4Pi raw images were linearly brightened, rescaled and linearly filtered by a sub-resolution mask using the image processing program ImageJ (Wayne Rasband, US National Institutes of Health, http://rsb.info.nih.gov/ij/).

A detailed description of 4Pi distance analysis has been published recently[22]. Briefly, the intensity profiles of the point spread function's main maximum in the two detection channels were independently fitted to an elliptical two-dimensional Gaussian function using a commercial plug-in for ImageJ (ILTracker, Ingo Lepper Software/Consulting) and the distance between the two centers was calculated.

For the distance analysis, only the nearest neighbors were taken into account. Additionally, for double staining for Syt1 and RIM1 plus RIM2, only patches that were diffraction limited in the red channel were analyzed.

Dual-color isoSTED imaging in the far-red. For isoSTED imaging, the PBS buffer was exchanged by a dilution series with 2,2-thiodiethanol (TDE) in PBS[49], finally resulting in an embedding medium of 97% (vol/vol) TDE in PBS. The sample was covered with a second coverslip that was sparsely coated with fluorescent beads (Crimson fluorescent microspheres, specified diameter 100 nm; Molecular Probes) to facilitate the initial alignment of the isoSTED nanoscope. Excitation of the dyes DY-480XL and KK114 was performed sequentially at wavelengths of 530 nm and 635 nm, respectively, using pulsed semiconductor lasers (PicoTA 530 and LDH-P-C 635b, each with PDL 800-B, PicoQuant) delivering <100-ps excitation pulses. These were synchronized with ~300-ps STED pulses originating from a mode-locked titanium:sapphire laser (Mai Tai, Spectra-Physics GmbH) operating at 79 MHz and at a wavelength of 775 nm, delivered and stretched by a single-mode optical fiber. Depending on availability, this device was replaced by a frequency-doubled fiber laser (ELP-5-775-DG, IPG Photonics Corporation) that emits 1-ns pulses at 20 MHz and at the same wavelength. In both cases, the time-averaged STED power in the sample was about 50 mW. Detection of the emission of both types of fluorophores was carried out in the 660–700 nm wavelength range using a photon-counting avalanche photodiode (PerkinElmer) and recorded in separate channels. Three-dimensional dual-color image stacks of synapses were nonlinearly deconvolved by applying 20 iterations of a Richardson–Lucy algorithm[50] to account for blurring effects of the imaging system. To this end, PSF estimates for both channels (DY-480XL and KK114) were obtained from the images of respective dye-tagged antibody clusters in remote areas of the sample. In the case of the Syt1–RIM1–RIM2 measurement, all signals within 60 nm of the coverslip were discarded to reduce the contribution of nonspecifically bound antibodies to the analysis.

Analysis of the spatial distribution of Syt1 versus Homer1. Correlation analysis was performed in Matlab independently on each of the marked regions (**Fig. 6b**) and evaluated in radial coordinates (d,θ) with

$$d = \sqrt{d_x^2 + d_y^2 + d_z^2)}$$

denoting the distance and $\theta = \mathrm{atan2}(d_x,d_y)$ denoting the azimuth angle between voxels. To estimate the orientation of the axon, the azimuth direction θ_{hom} of the local Homer1 run was obtained from the smoothed Homer1 intensity auto-correlation $H_{\mathrm{sm}}(d,\theta)$ as

$$\theta_{\mathrm{hom}} \equiv \mathrm{argmax}\left[\sum_d \mathrm{H_{sm}}(d,\theta)\right]$$

and represented by an arrow within the respective region (**Fig. 6b**). Subsequently, the Syt1-Homer1 cross-correlation $S(d,\theta)$ was calculated, taking into account all data values that exceeded a 10% lower threshold with regard to the global maximum. The result was transformed according to $S(d,\theta) \mapsto S(d,\alpha)$ with $\alpha = \theta - \theta_{\mathrm{hom}}$, and finally binned into a histogram (**Fig. 6d**).

48. Goslin, K. & Banker, G. Rat hippocampal neurons in low-density culture. in *Culturing Nerve Cells* 1st edn. (eds. Banker, G. & Goslin, K.) 251–281 (MIT Press, Cambridge, Massachusetts, USA, 1991).
49. Staudt, T., Lang, M.C., Medda, R., Engelhardt, J. & Hell, S.W. 2,2′-thiodiethanol: a new water soluble mounting medium for high resolution optical microscopy. *Microsc. Res. Tech.* **70**, 1–9 (2007).
50. Richardson, W.H. Bayesian-based iterative method of image restoration. *J. Opt. Soc. Am.* **62**, 55–59 (1972).